Elucidating the Thermal Decomposition of Dimethyl Methylphosphonate by Vacuum Ultraviolet (VUV) Photoionization: Pathways to the PO Radical, a Key Species in Flame-Retardant Mechan…

ARTICLE *in* CHEMISTRY - A EUROPEAN JOURNAL · NOVEMBER 2014

Impact Factor: 5.73 · DOI: 10.1002/chem.201404271

7 AUTHORS, INCLUDING:

Shuyu Liang
ETH Zurich
7 PUBLICATIONS **83** CITATIONS
SEE PROFILE

Patrick Hemberger
Paul Scherrer Institut
59 PUBLICATIONS **387** CITATIONS
SEE PROFILE

J. Levalois-Grützmacher
ETH Zurich
34 PUBLICATIONS **491** CITATIONS
SEE PROFILE

Sabyasachi Gaan
Empa - Swiss Federal Laboratories for Mate…
39 PUBLICATIONS **411** CITATIONS
SEE PROFILE

ChemPubSoc Europe

DOI: 10.1002/chem.201404271

CHEMISTRY
A European Journal
Full Paper

Phosphoryl Species

Elucidating the Thermal Decomposition of Dimethyl Methylphosphonate by Vacuum Ultraviolet (VUV) Photoionization: Pathways to the PO Radical, a Key Species in Flame-Retardant Mechanisms

Shuyu Liang,[a, b] Patrick Hemberger,*[c] N. Matthias Neisius,[a] Andras Bodi,[c] Hansjörg Grützmacher,[b] Joelle Levalois-Grützmacher,[b] and Sabyasachi Gaan*[a]

Abstract: The production of phosphoryl species (PO, PO_2, HOPO) is believed to be of great importance for efficient flame-retardant action in the gas phase. We present a detailed investigation of the thermal decomposition of dimethyl methylphosphonate (DMMP) probed by vacuum ultraviolet (VUV) synchrotron radiation and imaging photoelectron photoion coincidence (iPEPICO) spectroscopy. This technique provides a snapshot of the thermolysis process and direct evidence of how the reactive phosphoryl species are generated during heat exposure. One of the key findings of this work is that only PO is formed in high concentration upon DMMP decomposition, whereas PO_2 is absent. It can be concluded that the formation of PO_2 needs an oxidative environment, which is typically the case in a real flame. Based on the identification of products such as methanol, formaldehyde, and PO, as well as the intermediates O=P–CH_3, H_2C=P–OH, and H_2C=P(=O)H, supported by quantum chemical calculations, we were able to describe the predominant pathways that lead to active phosphoryl species during the thermal decomposition of DMMP.

Introduction

For a few decades, organophosphorus compounds (OPCs) have been extensively used as flame retardants (FRs) to inhibit or slow the spread of fire.[1] These compounds generally work in the gas phase, in the condensed phase, or in both, depending on the chemistry of the polymer matrix or substrate.[2] The condensed phase activities proceed by altering the thermal decomposition pathways of the polymer, by changing the viscosity of the system for heat retreat, or by forming a protective layer for flame/heat insulation. As reported by a series of previous studies, these activities can be studied by different analytical tools, such as thermogravimetric analysis (TGA), microscale combustion calorimetry (MCC), scanning electron microscopy (SEM), and X-ray photoelectron spectroscopy (XPS).[2h, 3]

[a] S. Liang, Dr. N. M. Neisius, Dr. S. Gaan
Additives and Chemistry, Advanced Fibers
Empa, Swiss Federal Laboratories for Materials Science
Lerchenfeldstrasse 5, 9014 St. Gallen (Switzerland)
E-mail: Sabyasachi.Gaan@empa.ch

[b] S. Liang, Prof. Dr. H. Grützmacher, Prof. Dr. J. Levalois-Grützmacher
Department of Chemistry and Applied Biosciences
ETH Zürich, 8093 Zürich (Switzerland)

[c] Dr. P. Hemberger, Dr. A. Bodi
Molecular Dynamics Group, Paul Scherrer Institute
WSLA/115, 5232 Villigen-PSI (Switzerland)
E-mail: patrick.hemberger@psi.ch

Supporting information for this article is available on the WWW under http://dx.doi.org/10.1002/chem.201404271.

Owing to the lack of suitable analytical techniques for selective and instantaneous analysis of the transient species formed in the thermal decomposition of OPCs, the elucidation of the gas-phase activity of phosphorous compounds is quite challenging. Important questions are still open, such as how individual bond energies in the flame-retardant molecules determine their fragmentation into gas-phase active products under thermal stress, what intermediates are formed under heat, and how flame-retardant efficiency can be maximized by targeted incorporation of specific functional groups into the flame retardant. Only a small number of studies have been performed to investigate the formation of PO_x reactive intermediates in the gas phase.[4]

Previously, we developed a series of novel OPCs for application in flexible polyurethane foams. Decomposition pathways of OPCs, which might explain their efficiency as a flame retardant, were studied by means of TGA, GC-MS, and direct insertion probe MS (DIP-MS).[5] Although the thermolysis of these compounds indicated a predominant activity in the gas phase, the results did not provide concrete evidence of the formation of reactive intermediates and the pathways thereto. Others have also proposed the formation of the PO radical by using TGA-MS (TGA coupled with a mass spectrometer), but these results are inconclusive.[6] In the long transfer line between the TGA apparatus and the mass spectrometer, the reactive intermediates decompose by wall reactions or can react with other species prior to detection.

These elusive intermediates can only be detected by coupling a sampling interface (sampling cones and differential

pumping stages) of a mass spectrometer directly with the reactive zones of, for example, flames and pyrolysis reactors.[7] Recently, such investigations have been carried out by using molecular beam mass spectrometry (MB-MS) techniques,[8] in which the reactive intermediates of trimethylphosphate were studied as flame retardants in syngas/air and propane flames. Therein, mechanisms for the inhibition were proposed. However, conventional electron-impact ionization allows neither fragmentation-free ionization nor a thorough isomer-selective detection of unimolecular decomposition products, which are crucial to understanding the gas-phase activity of FRs. This is the rationale behind using a soft ionization source, such as tunable vacuum ultraviolet (VUV) radiation, together with photoelectron spectroscopy—in particular, photoion mass-selected threshold photoelectron spectra (ms-TPES)—for isomer selection and a collision-reduced environment to suppress bimolecular reactions.

In this work, we have used a Chen-type[9] pyrolysis reactor to thermally decompose dimethyl methylphosphonate (DMMP; see Scheme 1) as a model for organophosphorus flame retardants.[10] Apart from matrix-isolation infrared spectroscopy,[11] imaging photoelectron photoion coincidence spectroscopy (iPEPICO)[12] has been found to be one of the most powerful tools in isomer-selective identification of complex reactive intermediates in synchrotron-based experiments and was also used in this study.[13]

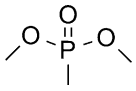

Scheme 1. The structure of dimethyl methylphosphonate (DMMP).

Our main objective was to identify the intermediates and the routes that generate the key phosphoryl radicals in the gas-phase flame-retardant action, with a special emphasis on the PO- and PO_2-generation capabilities of DMMP. DMMP has been the subject of only a few studies, mostly to develop models and mechanisms for the flame-inhibition action in combination with flat flame burners[8a,14] or theoretical investigations of the destruction of chemical warfare agents.[15] Identification of the product distribution as a function of pyrolysis temperature contributes to our understanding of fire suppression and helps us in proposing FR candidates with enhanced PO_x-release capabilities. Different computational chemistry approaches are applied in this study to augment the experimental data, including ab initio calculations to map the potential-energy surface of the neutral state, and locate transition states and minima to verify and validate the proposed decomposition mechanisms. Threshold photoelectron (TPE) spectra were simulated by applying a Franck–Condon approach and compared to the experimental results to unequivocally identify unknown elusive species.

Results and Discussion

Temperature-dependent photoionization mass spectra (TDPI-MS) of DMMP taken at 11 eV photon energy are presented in Figure 1. At temperatures below 700 °C (not shown in Figure 1) only *m/z* 79, 94, 109, and 124 are observed. These peaks can

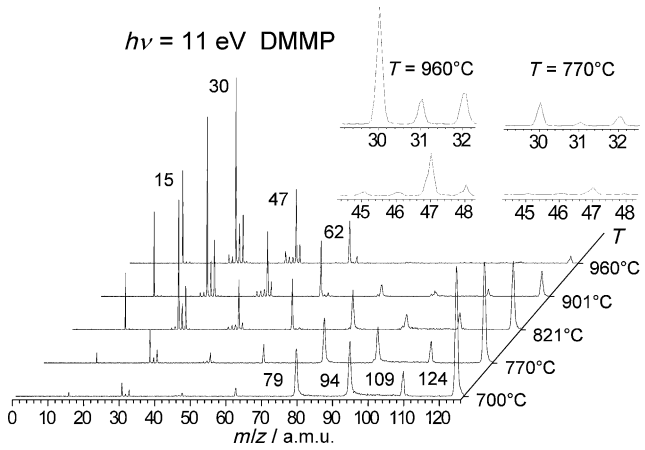

Figure 1. Temperature-dependent photoionization mass spectra of DMMP between 700 and 1000 °C, taken at $h\nu = 11$ eV.

be assigned to DMMP (*m/z* 124) and its dissociative photoionization channels, namely, methyl loss (*m/z* 109) and formaldehyde loss (*m/z* 94), followed by methyl loss (*m/z* 79). Since the methyl radical and formaldehyde counter fragments were not observed at 11 eV below a reactor temperature of 700 °C, it is evident that only dissociative photoionization occurred. In other words, neutral DMMP molecules were photoionized and the initially warm ones subsequently dissociated with the lower ionization energy fragment keeping the charge (see below). To elucidate this behavior in more detail, we recorded the ms-TPE spectra of the different *m/z* channels at room temperature and plotted the fractional ion abundances as a function of the photon energy in a breakdown diagram (Figure 2). The parent ion (*m/z* 124) starts to ionize dissociatively at around 10.6 eV with a formaldehyde-loss reaction to form *m/z* 94 (DMMP–CH_2O) after a hydrogen transfer. Above 12 eV, a direct methyl loss (*m/z* 109) from the parent ion (DMMP–CH_3) (see Figure 2) as well as a sequential methyl loss after the

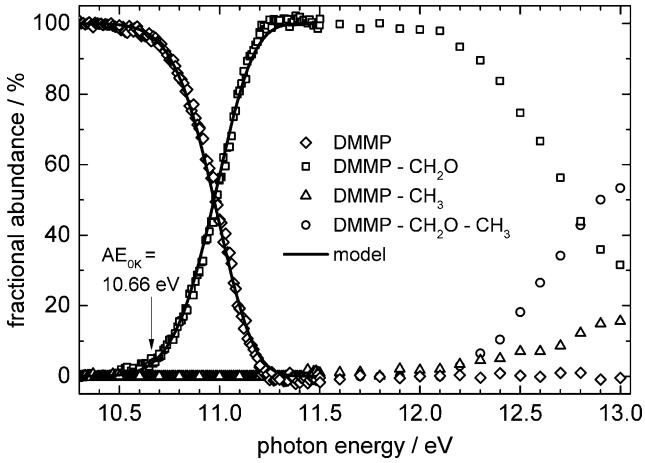

Figure 2. Room-temperature breakdown diagram of DMMP taken under effusive conditions. The points correspond to the measured fractional parent- and daughter-ion abundances in threshold photoionization, whereas the continuous lines indicate the statistical model with which the appearance energy has been determined (see the Supporting Information).

first formaldehyde loss (DMMP-CH_2O-CH_3, at *m/z* 79) can be observed. A detailed model for the first dissociation channel is given in the Supporting Information. In brief, by modeling[16] the dissociation rates, obtained as asymmetric daughter-ion time-of-flight (TOF) distributions, as well as the breakdown diagram of the first formaldehyde loss and taking into account the thermal energy distribution of the neutral state, a 0 K dissociative photoionization appearance energy of 10.66 eV can be determined. This compares well with the CBS-QB3 value of 10.45 eV.

It is generally accepted that the thermal-energy distribution of the neutral state is shifted into the ion manifold in threshold photoionization, which redshifts the appearance of the fragment ion and leads to a broadening of the breakdown diagram with increasing temperature. This effect can be directly observed in the TOF mass spectra depicted in Figure 3, in

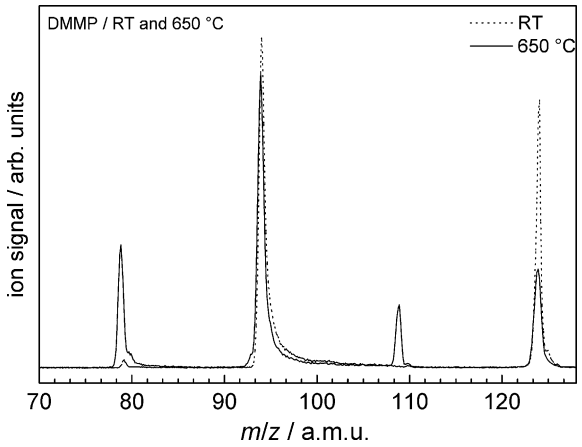

Figure 3. TOF mass spectra of DMMP at room temperature and at 650 °C taken at $h\nu = 12$ eV.

which two significant peaks at *m/z* 124, 94, and a minor one at 79 were observed at room temperature. When heating the reactor to 650 °C, two additional major peaks at *m/z* 79 and 109 appeared in the mass spectrum. However, neither spectrum showed peaks at lower mass units, thus ruling out the thermal decomposition of DMMP at these temperatures (and confirming the purity of the sample). Thus, one can conclude that the species at *m/z* 79, 96, and 109 correspond to the three dissociative photoionization channels below 13 eV and the precursor did not undergo thermal decomposition below 650 °C.

Equipped with this knowledge, we focused on the decomposition pathway of DMMP upon pyrolysis. Figure 1 shows that thermal decomposition of DMMP starts at around 700 °C and the formation of the most abundant products such as *m/z* 15, 30, 31, 32, 47, and 62 increases with higher reactor temperatures. These peaks can be easily assigned to the photoionization of the methyl radical (*m/z* 15), formaldehyde (*m/z* 30), and methanol (*m/z* 32), whereas the hydroxymethyl ion (*m/z* 31) is generated by means of dissociative ionization[17] of methanol. Interestingly, the ratio between methanol and formaldehyde changed upon increasing the reactor temperature. The question now arises as to whether methanol can form formaldehyde upon pyrolysis, or if there are parallel channels from DMMP that directly yield either methanol or formaldehyde. A further methanol pyrolysis experiment was carried out to investigate this. Temperature-dependent mass spectra of pure methanol were recorded and are shown in Figure 4. At higher

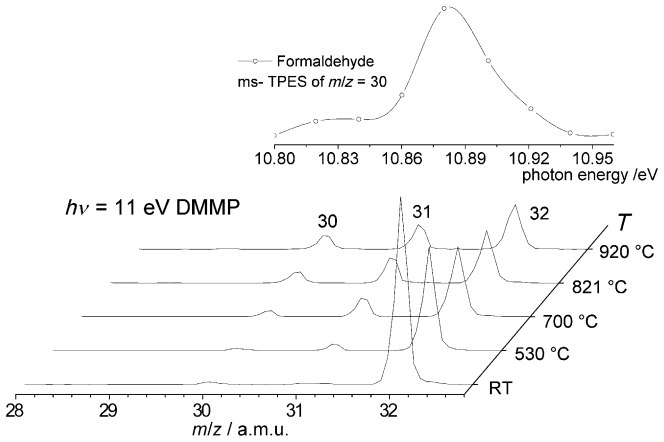

Figure 4. Temperature-dependent photoionization mass spectra of methanol. The room-temperature signal at *m/z* 30 is due to trace amounts of nitric oxide (NO) in the experiment, but *m/z* 30 ms-TPE spectra taken at high temperatures prove that methanol indeed yields formaldehyde upon decomposition.

temperatures the detected amount of methanol decreases slightly, whereas those of formaldehyde and hydroxymethyl ions increase. A mass-selected TPE spectrum that shows that thermally cracked methanol produces formaldehyde is shown as an inset in Figure 4. The hydroxymethyl (*m/z* 31)-to-methanol ratio in Figure 4 looks similar to that in Figure 1 as a function of temperature, and it is thus inferred that the peak for the hydroxymethyl ion in Figure 1 is completely due to the dissociative ionization of methanol instead of being a direct thermolysis product of DMMP.[17] Additionally, mass spectra below 10 eV do not show any indication of the formation of *m/z* 31, which originated from direct ionization of the radical species, with IE(hydroxymethyl) = 7.37 eV.[18] However, the ratios of formaldehyde to methanol are all less than one in Figure 4 and quite different from the ratios seen in Figure 1, namely, in excess of two and even increasing with higher temperatures. Therefore the formaldehyde indicated in Figure 1 was actually formed from two sources: from DMMP directly as well as from the DMMP decomposition product methanol. This is in contrast to the proposed decomposition mechanism by Yang et al.[15] In this detailed theoretical study, only high-energy H_2+CO channels are addressed computationally and not H_2CO production.

The assignment of the larger intermediates and products such as *m/z* 44, 46, 47, 62, and 64 is equivocal based on the photoion mass alone and has to rely on further speciation by mass-selected TPE spectra.

Identification of elusive species

A mass-selected TPE spectrum for the *m/z* 47 species was recorded at 950 °C with a step size of 5 meV. Hot and sequence bands are observed below the ionization energy of 8.38 ± 0.01) eV. To verify our assignment of this peak as PO, we conducted Franck–Condon simulations; the results are also shown in Figure 5. In addition, the spectral features are in excellent agreement with the PO photoelectron spectrum recorded by Dyke et al.,[19] and thus the TPE trace that coincides with *m/z* 47 photoions can be unambiguously assigned to the PO radical formed in the thermal decomposition of DMMP.

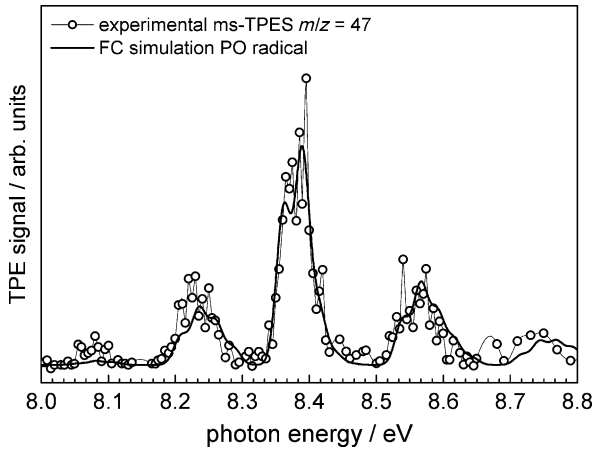

Figure 5. The TPE spectrum for the PO radical formed upon thermal decomposition of DMMP compared with a FC simulation. The obtained stick spectra were convoluted by a Gaussian function with a full width at half-maximum (fwhm) of 25 meV.

The ms-TPE spectrum of *m/z* 62 in Figure 6 shows four features at 9.3, 9.4, 9.5, and 9.6 eV. On the basis of the calculated ionization potentials and relative stabilities for six different $OPCH_3$ isomers, three candidates can be considered, namely,

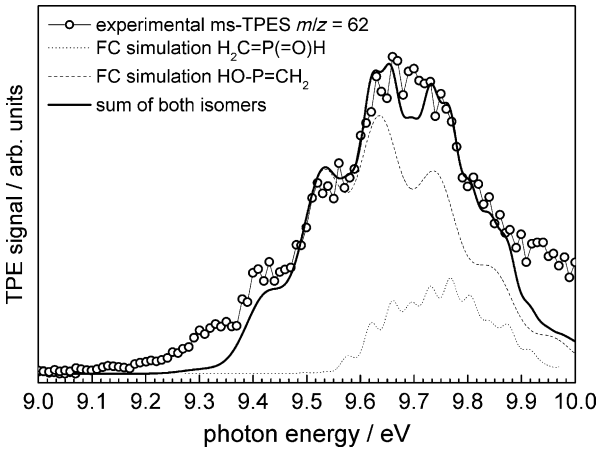

Figure 6. The threshold photoelectron spectrum (TPES) for the *m/z* 62 species formed upon thermal decomposition of DMMP compared with FC simulations. The simulated sticks were convoluted with Gaussian functions with fwhm = 81 and 30 meV for HO-P=CH_2 and H_2C=P(=O)H, respectively.

the tautomers HO-P=CH_2, O=P–CH_3, and methylene oxophosphorane, H_2C=P(=O)H, with calculated IE_{ad} values of 9.43, 9.52, and 9.61 eV, respectively (CBS-QB3 values). Franck–Condon simulations using the calculated ionization energies show that the features in Figure 6 can best be explained by a combination of both of the HO-P=CH_2 (dashed line) and H_2C=P(=O)H (dotted line) isomers. Thus, the *m/z* 62 peak is confirmed to be a mixture of at least two isomers, HO-P=CH_2 and H_2C=P(=O)H. The deviations below 9.3 and above 9.9 eV could be attributed to strong hot and sequence band contributions, but could also be due to the presence of the thermodynamically most stable isomer (see Figure 7) O=P–CH_3, of which the spectrum

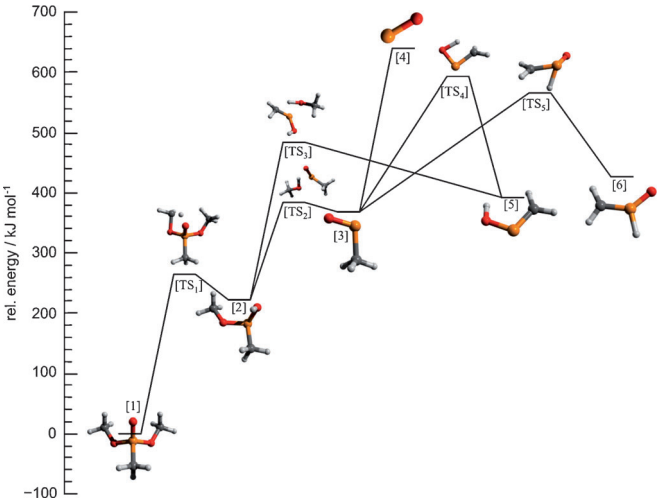

Figure 7. CBS-QB3 energy diagram for the thermal decomposition of DMMP in pathway 1. For the methyl loss to yield the PO radical, no transition state has been found on the singlet or on the triplet surface.

probably consists of broad bands because of the large geometry change and high amplitude motions upon ionization, and could not be simulated within the harmonic oscillator framework.

Minor products and intermediates such as *m/z* 44, 46, and 64 can be identified according to their mass-selected photoelectron spectra by using CBS-QB3-calculated ionization energies, as summarized in Table 1 and the Supporting Information. Since only trace amounts of these species were identified, they are not considered in the thermal-decomposition mechanism discussed below.

Table 1. Calculated and experimentally determined ionization energies of minor byproducts formed in traces during DMMP decomposition.

m/z	IE_{ad} (CBS-QB3) [eV]	IE_{ad} (exptl) [eV]	Assignment
44	10.79	10.82	HC–C≡P
46	9.98	≈9.9	HP=CH_2
64	10.88	≈10.8	O=POH

Mechanism of PO formation

It is generally believed that the gas-phase activity of flame retardants is caused by the release of phosphoryl (PO and PO_2) species.[4b,d] It is therefore crucial to understand how these elusive PO_x radicals are generated from their organophosphorous precursors. Here we will show that, based on the observed products and intermediates and supported by quantum chemical calculations, it is possible to derive a pathway for the unimolecular decomposition of DMMP.

As discussed in the context of the temperature-dependent mass spectra in Figure 1, both methanol and formaldehyde are formed at similar temperatures, which leads us to the assumption of at least two parallel pathways. Together with a comprehensive CBS-QB3 analysis of the potential-energy surface, we propose two predominant decomposition pathways, which proceed in parallel above a 700 °C reactor temperature. Pathway 1 (Figure 7) begins with a hydrogen transfer (TS_1) from one of the methoxy groups to the oxygen located at the phosphorous with a 260 kJ mol^{-1} activation energy. This is the rate-determining step in the formaldehyde loss reaction to form the intermediate $HOP(CH_3)(OCH_3)$ [2]. For the sake of clarity, the detailed mechanism for formaldehyde loss is only shown in Figure S4 in the Supporting Information. The transition structure TS_1 in fact leads to a three-membered P-O-CH_2 ring as was proposed by Yang et al.[15] The ring intermediate is, however, very short-lived, because it can open by hydrogen transfer from the P-O-H group to the oxygen of the three-membered ring, thus yielding an HO–CH_2 group, which is about 130 kJ mol^{-1} more stable than the three-membered ring. Afterwards, formaldehyde is released and [2] is formed over a transition state with an activation barrier of 150 kJ mol^{-1}. The *m/z* 94 ms-TPE spectrum, taken at lower pyrolysis temperatures (700–800 °C), did not contain spectral features that belong to species [2] with a calculated IE_{ad} of 8.13 eV. A signal in this mass channel was exclusively observed above 10 eV, which is assigned to redshifted dissociative ionization due to thermal effects. Thus, it is evident that this intermediate undergoes further decomposition instantaneously.

Another hydrogen transfer [TS_2] can take place from the hydroxyl group to the remaining methoxy function of [2], which yields methanol and OP–CH_3 [3] after dissociation with an activation energy of 160 kJ mol^{-1}. However, based on the ms-TPES in Figure 5, dominated by the HO-P=CH_2 and H_2C=P(=O)H species, it seems that this species is of minor importance. This finding can be explained by methyl radical loss from O=P–CH_3, which generates the PO [4] radical at a calculated reaction energy of 270 kJ mol^{-1} but without a reverse barrier, and completes the proposed mechanism.

In structure [2], a hydrogen can also be shifted from the methyl group to the methoxy group over the transition structure [TS_3], a process parallel to the methanol loss, and with a higher activation energy, thereby resulting in a second methanol-loss channel to form isomer HO-P=CH_2 [5]. This is the most prominent isomer in the mass-selected TPE spectrum (Figure 5). This isomer can equilibrate over a transition state of 200 kJ mol^{-1} [TS_4] with O=P–CH_3 [3]. Another isomer, namely, H_2C=P(=O)H [6], can also be formed at an activation energy of 200 kJ mol^{-1} from [3] over transition structure [TS_5] and contribute to the equilibrium, which is accessible below the barrier of the PO radical formation. Since O=P–CH_3 is the most stable among these tautomers and is expected to have the largest abundance in the mixture, and thus the largest contribution to the TPE signal. However, the spectrum (Figure 6) is dominated by the other two isomers, which warrants an explanation.

An equilibrium among O=P–CH_3 [3], HO–P=CH_2 [5], and H_2C=P(=O)H [6] is believed to come forth as a result of the small energy spacing between them and thanks to activation barriers surmountable at the reaction temperature. Among them, only O=P–CH_3 can continue to subtract a methyl group irreversibly and generate PO radicals. Thus, it acts as a $OPCH_3$ sink and will consume the other two isomers too. When looking at the reactor-temperature-dependent pyrolysis breakdown diagram among the species *m/z* 62, 47, and 15 (Figure 8), it is evident that *m/z* 62 diminishes, whereas the latter two increase simultaneously. Such a trend confirms that the O=P–CH_3 decomposition channel yields PO and methyl radicals. However, owing to the tight and relatively energetic transition states between these isomers, the depletion of HO-P=CH_2 and CH_2=P(=O)H species in the isomer equilibrium might not be completed within the pyrolysis time, typically a few hundred microseconds, and thus some of these species leave the reactor and undergo cooling in the molecular beam without being isomerized to O=P–CH_3 for further PO production. Methyl loss from [3], however, is expected to be fast in the absence of a reverse barrier, and once O=P–CH_3 has sufficient internal energy to dissociate, it will do so promptly.

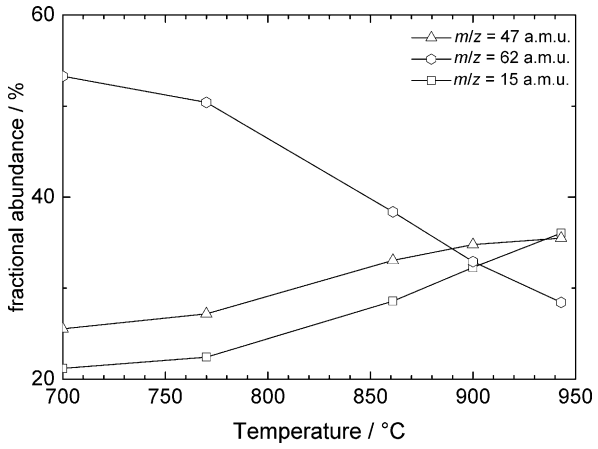

Figure 8. Temperature-dependent pyrolysis breakdown diagram for *m/z* 62, 47, and 15 obtained at $h\nu = 11$ eV from photoionization mass spectra.

As mentioned above, a second pathway might also exist at an activation energy of approximately 300 kJ mol^{-1} to proceed over a four-membered transition structure [TS_6], to yield methanol and [7] (Figure 9), which is the lowest-energy pathway also proposed by Yang et al.[15] As compared to the initial loss of formaldehyde in pathway 1, that of methanol to form the methoxy methylene oxophosphorane H_2C=P(=O)(OCH_3) [7] with a computed IE_{ad}(CBS-QB3) = 8.85 eV in pathway 2 is be-

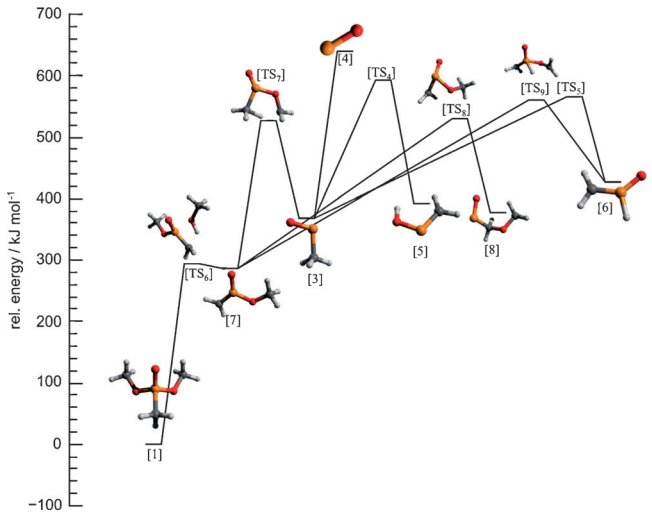

Figure 9. CBS-QB3 energy diagram for the thermal decomposition of DMMP in pathway 2.

lieved to have a similar activation energy and can thus also play a role in the early decomposition of DMMP. Owing to the insufficient signal at *m/z* 92 and the large dissociative ionization signal at *m/z* 94, this first intermediate could not be observed, which is also explained by the fact that this species readily decomposes further. To cross the next transition structure [TS_7], which leads to the loss of formaldehyde and to yield the O=P–CH_3 isomer [3], an activation energy of around 230 kJ mol^{-1} is required. Directly from [7] another parallel pathway proceeds with a hydrogen shift from the methoxy function to the phosphorous to yield the H_2C=P(=O)H [6] isomer, followed by a second hydrogen shift to give O=P–CH_3 [3] (equilibrium through TS5 in Figure 7). In addition, [7] might also undergo a methoxy shift [TS_8] over a barrier of 240 kJ mol^{-1} to yield O=P-CH_2-O-CH_3 [8] and further provide PO species after a homolytic cleavage of the P–C bond. Alternatively, the intramolecular hydrogen transfer from the O–CH_3 group of [8] to its methylene group under a concomitant loss of formaldehyde might also occur to yield O=P–CH_3 [3], which suffers from homolytic bond scission to PO and CH_3.

Again, the residence time in the pyrolysis reactor is too short to equilibrate the molecule completely to O=P–CH_3, and thus fingerprints for the other two energetically higher-lying isomers are only observed.

In summary, both pathways 1 and 2 have similar activation energies for the generation of PO and methyl radicals and proceed either through formaldehyde loss and subsequent methanol-loss reaction or vice versa. The experimental evidence for H_2CO production was backed up by the computed energetics, which showed that instead of the high activation energy H_2 + CO channel,[15] H_2CO can be produced more readily. No PO_2 signal was detected, which is one of the key findings in this study. The absence of PO_2 means that there is no direct pathway to this molecule under unimolecular conditions and that its formation involves further oxidation of PO or another intermediate under combustion conditions. Indeed, it is known in the literature that in hydrogen/oxygen and methane/oxygen/N_2 premixed flat flames, PO_2 and $HOPO_2$ intermediates are observed and result from the destruction of DMMP by means of mostly bimolecular reactions with flame species such as H and OH.[8a,14a,20] A mechanism for the formation of PO radicals was determined by Korobeinichev et al.[20b] However, when the flame retardant is incorporated in a polymer matrix, gas-phase action in a flame will start by thermolysis in oxygen-poor regions at the polymer/flame interface. It is at these initial stages of flame-retardant action that unimolecular decomposition processes will play an important and yet unstudied role relative to typical premixed flames, which are rarely seeded with flame retardants in real life.

Conclusion

The thermal-decomposition mechanism of dimethyl methylphosphonate (DMMP) was probed by vacuum ultraviolet (VUV) synchrotron radiation and imaging photoelectron photoion coincidence (iPEPICO) spectroscopy by recording temperature-dependent photoionization mass spectra. In conjunction with the room-temperature ms-TPES and the DMMP breakdown diagram, it was possible to distinguish between the mass-spectrum peaks owing to dissociative photoionization and the thermolysis products. Furthermore, the major thermolysis products could be identified isomer-selectively by using their photoelectron fingerprint together with Franck–Condon simulations. TDPI-MS analyses show that thermal decomposition of DMMP starts at around 700 °C, and the abundances of the products and intermediates at *m/z* 15, 30, 31, 32, 47, and 62 increase swiftly with increasing temperature.

We found that the residence time in the pyrolysis reactor was sufficient for the first-tier intermediates to quantitatively dissociative further, and only the PO radicals and their immediate precursors could be identified together with the organic dissociation side products. To confirm the computational results and get a glimpse into the first microseconds of the thermolysis, rethermalization of the intermediates should be further curtailed by using a reactor with an even smaller residence time. The complete absence of the PO_2 signal nevertheless proves its oxidative production in flames after initial thermolysis of the flame retardant. The roles of three different CH_3OP isomers, the tautomers H_2C=P–OH, H_2C=P(=O)H, and the constitutional isomer O=P–CH_3, have been discussed.

By employing quantum chemical calculations, we have determined two predominant pathways that generate the active phosphoryl species during thermal decomposition of DMMP. Both pathways start either with methanol or formaldehyde loss as the first step, which are followed by subsequent formaldehyde or methanol loss to yield the intermediate $OPCH_3$ isomers. These three isomers form an equilibrium under the pyrolysis conditions and only the O=P–CH_3 isomer can generate methyl and PO radicals upon further decomposition. A new unimolecular formaldehyde loss channel could be identified from DMMP, which was not foreseen in a theoretical study,[15] thus showing that even the most careful computational approaches might be incomplete without experimental data to rely on.

Experimental and Computational Methods

The experiments were conducted at the VUV beamline of the Swiss Light Source at the Paul Scherrer Institute in Villigen, Switzerland. Both the beamline and endstation have been described in detail elsewhere.[12,21] In brief, the X04DB bending magnet generates synchrotron radiation, and three optical elements (collimating mirror, monochromator, and focusing mirror) transport the light downstream to the ionization chamber of the iPEPICO endstation. A mixture of Kr/Ar/Ne at a pressure of 10 mbar was used in a differentially pumped gas filter to suppress the higher order radiation, which is also diffracted by the grating. A photon energy resolution of 5–10 meV was achieved by using either the 600 or the 150 lines mm^{-1} grating, as calibrated on argon autoionization lines.

The iPEPICO endstation was employed to study the photoionization of products as well as intermediate species in the gas phase. This technique allowed the selective detection of threshold photoelectrons in coincidence with a photoion *m/z* channel by using a Wiley–McLaren time-of-flight (TOF) mass spectrometer for the ions and a velocity map imaging setup[22] for electron detection. With regards to the measurement of TPE spectra to identify individual *m/z* peaks, only the central part (typically 5–10 meV) of the electron image was taken into account, and the hot-electron background was subtracted following the method by Sztáray and Baer.[23]

A flange equipped with a molecular beam source and a silicon carbide (SiC) tubular reactor was mounted in the source chamber. The temperature of the SiC tube was controlled by an external power supply and measured by a type-C thermocouple with ± 100 K accuracy.[11b] To avoid self-reactions, the sample was diluted with argon before entering the pyrolysis reactor. After leaving the reactor, the molecular beam was skimmed (2 mm, Beam Dynamics Inc.) before entering the ionization chamber, in which it was ionized by the incident VUV radiation.

DMMP was purchased from Sigma–Aldrich, Switzerland, distilled before use, and seeded in argon (0.4 bar) in a bubbler, which corresponded to a concentration of 0.33%, and expanded into the pyrolysis reactor. Low sample dilution was crucial to reduce bimolecular reactions. Methanol was supplied by VWR Switzerland and was diluted to 0.5% in argon prior to use. Mass spectra and mass-selected TPE spectra were taken at different temperatures (from room temperature to 1000 °C) and typically averaged for 60–120 s per data point.

The Gaussian 09[24] software suite was used to conduct the quantum chemical calculations by applying the B3LYP functional and the 6-311++G(d,p) basis set to calculate equilibrium geometries and force-constant matrixes as used in the Franck–Condon simulations (ezSpectrum OSX, pgopher).[25] The line spectrum was subsequently convoluted with a Gaussian function for comparison with the experimental photoion mass-selected TPE spectrum. Reliable ionization energies and relative energies for intermediates, transition states, and products were calculated using the CBS-QB3 method.[26] All reported electronic energies were corrected by the zero-point energy.

Acknowledgements

The measurements were carried out at VUV beamline of the Swiss Light Source, Paul Scherrer Institut (PSI). Quantum chemical calculations were performed at Merlin4 cluster at PSI. P.H. and A.B. gratefully acknowledge support by Swiss Federal Office for Energy (BFE Contract Number 101969/152433).

Keywords: ab initio calculations · organophosphorus compounds · photoelectron spectroscopy · radicals · thermochemistry

[1] a) D. W. Edward in *Handbook of Organophosphorus Chemistry* (Ed.: R. Engel), Polymer Research Institute, Polytechnic University, Brooklyn, **1992**, Chapter 14 ; b) B. Li, Z. Zhan, H. Zhang, C. Sun, *J. Vinyl Technol.* **2014**, *20*, 10–15; c) I. Jirasutsakul, B. Paosawatyanyong, W. Bhanthumnavin, *Prog. Org. Coat.* **2013**, *76*, 1738–1746; d) O. B. Mauerer, D. Ilona, *Spec. Chem. Mag.* **2007**, *27*, 34–35, ISSN:0262–2262; e) C. Zhou, R. W. AVAKIAN, in PCT Int. Appl. WO2013US59217 20130911 Polyone Corporation, USA, **2014**.

[2] a) D. Hoang, J. Kim, B. N. Jang, *Polym. Degrad. Stab.* **2008**, *93*, 2042–2047; b) A. König, E. Kroke, *Fire Mater.* **2012**, *36*, 1–15; c) G. Camino, L. Costa, L. Trossarelli, *Polym. Degrad. Stab.* **1985**, *12*, 203–211; d) G. Camino, L. Costa, G. Martinasso, *Polym. Degrad. Stab.* **1989**, *23*, 359–376; e) B. Schartel, *Materials* **2010**, *3*, 4710–4745; f) G. Camino, G. Martinasso, L. Costa, *Polym. Degrad. Stab.* **1990**, *27*, 285–296; g) M. Thirumal, N. K. Singha, D. Khastgir, B. S. Manjunath, Y. P. Naik, *J. Appl. Polym. Sci.* **2010**, *116*, 2260–2268; h) A. Gentilhomme, M. Cochez, M. Ferriol, N. Oget, J. L. Mieloszynski, *Polym. Degrad. Stab.* **2005**, *88*, 92–97.

[3] a) C. N. J. Kim, *Macromol. Res.* **2008**, *16*, 620–625; b) S. Bernhard, H. R. Kristin, B. Martin, in *Fire and Polymers VI: New Advances in Flame Retardant Chemistry and Science, Vol. 1118*, American Chemical Society, **2012**, pp. 15–36; c) W. Zhang, X. Li, R. Yang, *Polym. Degrad. Stab.* **2014**, *99*, 298–303; d) H. Vahabi, C. Longuet, L. Ferry, G. David, J.-J. Robin, J.-M. Lopez-Cuesta, *Polym. Int.* **2012**, *61*, 129–134.

[4] a) A. Twarowski, *Combust. Flame* **1993**, *94*, 91–107; b) A. Twarowski, *Combust. Flame* **1996**, *105*, 407–413; c) A. Twarowski, *Combust. Flame* **1995**, *102*, 41–54; d) A. Granzow, *Acc. Chem. Res.* **1978**, *11*, 177–183.

[5] a) S. Liang, M. Neisius, H. Mispreuve, R. Naescher, S. Gaan, *Polym. Degrad. Stab.* **2012**, *97*, 2428–2440; b) M. Neisius, S. Liang, H. Mispreuve, S. Gaan, *Ind. Eng. Chem. Res.* **2013**, *52*, 9752–9762.

[6] a) A. König, E. Kroke, *Polym. Adv. Technol.* **2011**, *22*, 5–13; b) J. Feng, J. Hao, J. Du, R. Yang, *Polym. Degrad. Stab.* **2012**, *97*, 605–614.

[7] Y. Li, F. Qi, *Acc. Chem. Res.* **2009**, *42*, 68–78.

[8] a) O. P. Korobeinichev, T. A. Bolshova, V. M. Shvartsberg, A. A. Chernov, *Combust. Flame* **2001**, *125*, 744–751; b) V. M. Shvartsberg, A. G. Shmakov, T. A. Bolshova, O. P. Korobeinichev, *Energy Fuels* **2012**, *26*, 5528–5536.

[9] D. W. Kohn, H. Clauberg, P. Chen, *Rev. Sci. Instrum.* **1992**, *63*, 4003–4005.

[10] F. Feng, L. Qian, *Polym. Compos.* **2014**, *35*, 301–309.

[11] a) A. M. Scheer, C. Mukarakate, D. J. Robichaud, M. R. Nimlos, H.-H. Carstensen, G. Barney Ellison, *J. Chem. Phys.* **2012**, *136*, 044309; b) A. M. Scheer, C. Mukarakate, D. J. Robichaud, M. R. Nimlos, G. B. Ellison, *J. Phys. Chem. A* **2011**, *115*, 13381–13389; c) M. W. Jarvis, J. W. Daily, H.-H. Carstensen, A. M. Dean, S. Sharma, D. C. Dayton, D. J. Robichaud, M. R. Nimlos, *J. Phys. Chem. A* **2011**, *115*, 428–438.

[12] A. Bodi, M. Johnson, T. Gerber, Z. Gengeliczki, B. Sztáray, T. Baer, *Rev. Sci. Instrum.* **2009**, *80*, 034101.

[13] a) P. Oßwald, P. Hemberger, T. Bierkandt, E. Akyildiz, M. Köhler, A. Bodi, T. Gerber, T. Kasper, *Rev. Sci. Instrum.* **2014**, *85*, 025101; b) V. B. F. Custodis, P. Hemberger, Z. Ma, J. A. van Bokhoven, *J. Phys. Chem. B* **2014**; c) P. Hemberger, A. J. Trevitt, E. Ross, G. da Silva, *Chem. Phys. Lett.* **2013**, *4*, 2546–2550; d) A. Bodi, P. Hemberger, D. L. Osborn, B. Sztáray, *Chem. Phys. Lett.* **2013**, *4*, 2948–2952; e) F. Holzmeier, M. Lang, K. Hader, P. Hemberger, I. Fischer, *J. Chem. Phys.* **2013**, *138*, 214310; f) M. Steinbauer, P. Hemberger, I. Fischer, A. Bodi, *ChemPhysChem* **2011**, *12*, 1795–1797; g) F. Holzmeier, M. Lang, P. Hemberger, A. Bodi, M. Schäfer, R. D. Dewhurst, H. Braunschweig, I. Fischer, *Chem. Eur. J.* **2014**, *20*, 9683–9692; h) P. Hemberger, A. Bodi, T. Gerber, M. Würtemberger, U. Radius, *Chem. Eur. J.* **2013**, *19*, 7090–7099; i) P. Hemberger, A. J. Trevitt, T. Gerber, E. Ross, G. da Silva, *J. Phys. Chem. A* **2014**.

[14] a) J. H. Werner, T. A. Cool, *Combust. Flame* **1999**, *117*, 78 – 98; b) M. A. MacDonald, F. C. Gouldin, E. M. Fisher, *Combust. Flame* **2001**, *124*, 668 – 683.
[15] L. Yang, R. M. Shroll, J. Zhang, U. Lourderaj, W. L. Hase, *J. Phys. Chem. A* **2009**, *113*, 13762 – 13771.
[16] B. Sztáray, A. Bodi, T. Baer, *J. Mass Spectrom.* **2010**, *45*, 1233 – 1245.
[17] S. Borkar, B. Sztaray, A. Bodi, *Phys. Chem. Chem. Phys.* **2011**, *13*, 13009 – 13020.
[18] J. M. Dyke, *J. Chem. Soc. Faraday Trans.* **1987**, *83*, 69 – 87.
[19] J. M. Dyke, A. Morris, A. Ridha, *J. Chem. Soc. Faraday Trans.* **1982**, *78*, 2077 – 2082.
[20] a) O. P. Korobeinichev, S. B. Ilyin, V. M. Shvartsberg, A. A. Chernov, *Combust. Flame* **1999**, *118*, 718 – 726; b) O. P. Korobeinichev, S. B. Ilyin, T. A. Bolshova, V. M. Shvartsberg, A. A. Chernov, *Combust. Flame* **2000**, *121*, 593 – 609; c) M. F. M. Nogueira, E. M. Fisher, *Combust. Flame* **2003**, *132*, 352 – 363; d) P. A. Glaude, C. Melius, W. J. Pitz, C. K. Westbrook, *Proc. Combust. Inst.* **2002**, *29*, 2469 – 2476.
[21] M. Johnson, A. Bodi, L. Schulz, T. Gerber, *Nucl. Instrum. Methods Phys. Res. Sect. A* **2009**, *610*, 597 – 603.
[22] *Imaging in Molecular Dynamics* (Ed.: B. J. Whitaker), Cambridge University Press, Cambridge, **2003**.
[23] B. Sztáray, T. Baer, *Rev. Sci. Instrum.* **2003**, *74*, 3763.
[24] Gaussian 09, Revision C.01, M. J. Frisch, G. W. Trucks, H. B. Schlegel, G. E. Scuseria, M. A. Robb, J. R. Cheeseman, G. Scalmani, V. Barone, B. Mennucci, G. A. Petersson, H. Nakatsuji, M. Caricato, X. Li, H. P. Hratchian, A. F. Izmaylov, J. Bloino, G. Zheng, J. L. Sonnenberg, M. Hada, M. Ehara, K. Toyota, R. Fukuda, J. Hasegawa, M. Ishida, T. Nakajima, Y. Honda, O. Kitao, H. Nakai, T. Vreven, J. A. Montgomery, Jr., J. E. Peralta, F. Ogliaro, M. Bearpark, J. J. Heyd, E. Brothers, K. N. Kudin, V. N. Staroverov, R. Kobayashi, J. Normand, K. Raghavachari, A. Rendell, J. C. Burant, S. S. Iyengar, J. Tomasi, M. Cossi, N. Rega, J. M. Millam, M. Klene, J. E. Knox, J. B. Cross, V. Bakken, C. Adamo, J. Jaramillo, R. Gomperts, R. E. Stratmann, O. Yazyev, A. J. Austin, R. Cammi, C. Pomelli, J. W. Ochterski, R. L. Martin, K. Morokuma, V. G. Zakrzewski, G. A. Voth, P. Salvador, J. J. Dannenberg, S. Dapprich, A. D. Daniels, Ö. Farkas, J. B. Foresman, J. V. Ortiz, J. Cioslowski, D. J. Fox, Gaussian, Inc., Wallingford CT, **2009**.
[25] a) ezSpectrum http://iopenshell.usc.edu/downloads, A. Mozhayskiy, A. I. Krylov, **2014**; b) PGOPHER, a Program for Simulating Rotational Structure, C. M. Western, http://pgopher.chm.bris.ac.uk, University of Bristol.
[26] a) J. A. Montgomery, M. J. Frisch, J. W. Ochterski, G. A. Petersson, *J. Chem. Phys.* **1999**, *110*, 2822 – 2827; b) J. A. Montgomery, M. J. Frisch, J. W. Ochterski, G. A. Petersson, *J. Chem. Phys.* **2000**, *112*, 6532 – 6542.

Received: July 7, 2014
Published online on November 20, 2014